

Patient-Specific Wall Stress Analysis in Cerebral Aneurysms Using Inverse Shell Model

XIANLIAN ZHOU,¹ MADHAVAN L. RAGHAVAN,² ROBERT E. HARBAUGH,³ and JIA LU¹

¹Department of Mechanical and Industrial Engineering, Center for Computer Aided Design, The University of Iowa, Iowa City, IA 52242, USA; ²Department of Biomedical Engineering, The University of Iowa, Iowa City, IA 52242, USA; and ³Departments of Neurosurgery, and Engineering Science and Mechanics, Penn State University, Hershey, PA 17033, USA

(Received 21 April 2008; accepted 6 November 2009; published online 21 November 2009)

Abstract—Stress analyses of patient-specific vascular structures commonly assume that the reconstructed *in vivo* configuration is stress free although it is in a pre-deformed state. We submit that this assumption can be obviated using an inverse approach, thus increasing accuracy of stress estimates. In this paper, we introduce an inverse approach of stress analysis for cerebral aneurysms modeled as nonlinear thin shell structures, and demonstrate the method using a patient-specific aneurysm. A lesion surface derived from medical images, which corresponds to the deformed configuration under the arterial pressure, is taken as the input. The wall stress in the given deformed configuration, together with the unstressed initial configuration, are predicted by solving the equilibrium equations as opposed to traditional approach where the deformed geometry is assumed stress free. This inverse approach also possesses a unique advantage, that is, for some lesions it enables us to predict the wall stress without accurate knowledge of the wall elastic property. In this study, we also investigate the sensitivity of the wall stress to material parameters. It is found that the in-plane component of the wall stress is indeed insensitive to the material model.

Keywords—Cerebral aneurysms, Wall stress, Patient-specific analysis, Inverse elastostatics, Inverse shell analysis.

INTRODUCTION

Assessing the rupture risk of cerebral aneurysm (CA) has been an area of considerable interest for many years. The size of the lesion is traditionally considered as a main prognostic indicator, with factors such as age, gender, and smoking history being subjectively taken into consideration. However, data from large population studies like the International Study of Unruptured Intracranial Aneurysms suggest that

size is not a reliable index of rupture risk.¹ Recently, other physics-based indicators, in particular the mechanical stress, have been submitted based on the premise that aneurysms rupture when the local wall stress exceeds the tissue strength. Along this line of thinking, the mechanical behavior of cerebral aneurysms has received considerable attention in recent years.^{2,4,11,15,16,22–24}

While early investigations on aneurysm wall stress mostly focused on idealized lesions, recently the emphasis has shifted to patient-specificity in the attempt to predict the wall stress on a patient-specific basis. A common approach is to utilize patient-specific geometries derived from biomedical images but use reported population average wall properties. Most previous works, include one of our own,¹⁶ assumed the imaged geometry to be the initial stress-free configuration and proceeded to compute the wall stress under pressures using the standard forward method. It should be noted that the *in vivo* images of aneurysm correspond to a pre-deformed state due to the presence of arterial pressure. Ignoring the pre-deformation was certainly a limitation in the previous works and would inevitably result in some error in stress estimates. To address this limitation, the present authors have introduced the inverse elastostatic method^{12–14} in aneurysm mechanics. In the inverse approach, the image geometry is taken as a deformed configuration as it should be. The stress in the deformed state, along with an initial stress-free configuration, are determined from solving the equilibrium equations. It has been found that ignoring the pre-stretch tends to over-predict the wall stress. For abdominal aortic aneurysm, we reported a stress error margin of 13–17% within a reasonable range of material parameter variation.¹³ For cerebral aneurysm, the stress difference from these two approaches is expected to be smaller because the physiological deformation of cerebral aneurysms is normally smaller than that of

Address correspondence to Jia Lu, Department of Mechanical and Industrial Engineering, Center for Computer Aided Design, The University of Iowa, Iowa City, IA 52242, USA. Electronic mail: jia-lu@uiowa.edu, jialu@engineering.uiowa.edu

aortic aneurysms. Nevertheless, the existence of pre-deformation is a characteristic of aneurysm mechanics and its influence on stress prediction should be investigated.

The inverse approach has an even more important implication to patient-specific analysis. It is well-known that a pressurized thin-walled sac-like structure is statically determined, or at least approximately so, in the sense that the wall stress depends primarily on the *deformed* shape and the pressure but minimally on the material's elastic properties. This unique feature has been recognized and utilized in aneurysm mechanics. Analytical stress solutions have been derived for idealized aneurysms.^{3,5,24} For relatively deep lesions (which the height is comparable to the diameter), the stress in regions away from the neck is expected to be statically-determined. However, in the forward approach, the dependence on material property is implicit because the deformed geometry is yet to be determined. In contrast, the inverse approach is expected to sharply capture the “static stress” because the equilibrium analysis is carried out on the deformed geometry. This implies that for a certain groups of lesions the wall stress (to be precise, the in-plane components of the stress resultant) may be accurately predicted without accurate knowledge of patient-specific wall properties. In a recent work,¹⁴ the present authors reported a profound material insensitivity in membrane models of cerebral aneurysms. This unique characteristic of inverse approach is significant for patient-specific analysis, because the current diagnostic tools are unable to obtain patient-specific wall properties.

The analysis in Lu *et al.*¹⁴ assumed that the aneurysm wall is a thin membrane that does not sustain flexure bending and transverse shear. This assumption is inadequate for thin structures having concave surface regions. Due to lack of bending, a membrane theory precludes deformations that ripple the wall. The membrane assumption places a rather severe limitation on the application to aneurysms. Realistic cerebral aneurysms often have undulated surfaces even when pressurized. The inverse membrane simulation in Lu *et al.*,¹⁴ although possessing a remark feature, is not suited to general patient-specific applications.

In this paper, we further eliminate the restrictions on surface shape by introducing an inverse nonlinear shell analysis for cerebral aneurysms. The inverse formulation of stress resultant shell theory recently introduced in Zhou and Lu³² is utilized. For the sake of completeness, a brief description of the inverse shell is given in “Method” section. An image-reconstructed cerebral aneurysm is considered. Using an anisotropic Fung material model reported for cerebral aneurysm

tissue, we predicted the initial geometry and the stress resultants in the given deformed state. To investigate static determinacy, we performed material sensitivity analyses by comparing the in-plane stress resultant predicted from two families of material models with drastically different symmetry characteristics and large variations of stiffness parameters. We demonstrate that, despite the consideration of bending and the transverse shear, the in-plane stress resultant remains insensitive to the material parameters. The in-plane stress, which is the major index in rupture assessment, may still be estimated without accurate knowledge of the wall elastic parameters.

METHOD

Stress Resultant Shell

A shell is a thin material body in which the thickness is much smaller than the other dimensions. The theories of shell have been developed mainly along two approaches, the continuum theory and the direct (stress resultant) theory.^{18,27} In the latter, a shell structure is modeled as a deformable surface equipped with a director field. The initial (undeformed) configuration is

$$\mathcal{R} := \left\{ \mathbf{X} \in \mathbb{R}^3 \mid \mathbf{X} = \Phi + \xi \mathbf{D}, \xi \in \left[-\frac{h}{2}, \frac{h}{2} \right] \right\}, \quad (1)$$

where Φ and \mathbf{D} are the positions of material points in the mid-surface and the reference director field, respectively, and both are functions of the surface coordinates (ξ^1, ξ^2) . The current, or deformed configuration is specified by

$$\mathcal{C} := \left\{ \mathbf{x} \in \mathbb{R}^3 \mid \mathbf{x} = \boldsymbol{\varphi} + \xi \mathbf{d}, \xi \in \left[-\frac{h}{2}, \frac{h}{2} \right] \right\}. \quad (2)$$

where $\boldsymbol{\varphi}$ and \mathbf{d} are the current mid-surface and the directors, and h is the current wall thickness.

The local deformation of the shell is described by the following deformation measures

$$\begin{aligned} a_{\alpha\beta} &:= \boldsymbol{\varphi}_{,\alpha} \cdot \boldsymbol{\varphi}_{,\beta}, & A_{\alpha\beta} &:= \Phi_{,\alpha} \cdot \Phi_{,\beta}, \\ \kappa_{\alpha\beta} &:= \boldsymbol{\varphi}_{,\alpha} \cdot \mathbf{d}_{,\beta}, & K_{\alpha\beta} &:= \Phi_{,\alpha} \cdot \mathbf{D}_{,\beta}, \\ \gamma_{\alpha} &:= \boldsymbol{\varphi}_{,\alpha} \cdot \mathbf{d}, & \Gamma_{\alpha} &:= \Phi_{,\alpha} \cdot \mathbf{D}, \end{aligned} \quad (3)$$

where $a_{\alpha\beta}$ and $A_{\alpha\beta}$ are components of surface metric tensors. Note that in this paper, the notation $(\cdot)_{,\alpha}$ indicates the partial derivative relative to the coordinate ξ^α , and the summation convention applies to the Greek indices which range from 1 to 2. The vectors $\mathbf{a}_\alpha = \boldsymbol{\varphi}_{,\alpha}$ at a material point form convected bases tangent to the surface, with $\mathbf{A}_\alpha = \Phi_{,\alpha}$ being the bases in the reference state. It is also convenient to describe the deformation in terms of the surface strain tensor $\boldsymbol{\varepsilon}$, the

relative curvature tensor ρ , and the transverse shear strain δ :

$$\begin{aligned}\boldsymbol{\varepsilon} &:= \varepsilon_{\alpha\beta} \mathbf{A}^\alpha \otimes \mathbf{A}^\beta = \frac{1}{2} (a_{\alpha\beta} - A_{\alpha\beta}) \mathbf{A}^\alpha \otimes \mathbf{A}^\beta, \\ \boldsymbol{\rho} &:= \rho_{\alpha\beta} \mathbf{A}^\alpha \otimes \mathbf{A}^\beta = (\kappa_{\alpha\beta} - K_{\alpha\beta}) \mathbf{A}^\alpha \otimes \mathbf{A}^\beta, \\ \boldsymbol{\delta} &:= \delta_\alpha \mathbf{A}^\alpha = (\gamma_\alpha - \Gamma_\alpha) \mathbf{A}^\alpha.\end{aligned}\quad (4)$$

The kinetics of the shell is formulated in terms of the stress resultant \mathbf{n} and stress couple $\tilde{\mathbf{m}}$. In relation to the 3D Cauchy stress $\boldsymbol{\sigma}$ they are defined as

$$\mathbf{n}^\alpha := \frac{1}{\sqrt{a}} \int_{-\frac{h}{2}}^{\frac{h}{2}} \boldsymbol{\sigma} \mathbf{g}^\alpha j d\zeta, \quad \tilde{\mathbf{m}}^\alpha := \frac{1}{\sqrt{a}} \int_{-\frac{h}{2}}^{\frac{h}{2}} \zeta \boldsymbol{\sigma} \mathbf{g}^\alpha j d\zeta, \quad (5)$$

where $\sqrt{a} = \|\mathbf{a}_1 \times \mathbf{a}_2\|$ is the surface Jacobian, j is the 3D Jacobian of configuration mapping $\mathcal{R} \rightarrow \mathcal{C}$, and \mathbf{g}^α is the 3D contravariant basis vectors induced by the convected coordinates $(\xi^1, \xi^2, \xi^3 = \zeta)$. Note that the resultants contain an in-plane and a transverse component. To decompose the stress we write

$$\mathbf{n}^\alpha = n^{\alpha\beta} \mathbf{a}_\beta + q^\alpha \mathbf{d}, \quad \tilde{\mathbf{m}}^\alpha = \tilde{m}^{\alpha\beta} \mathbf{a}_\beta + \tilde{m}^{3\alpha} \mathbf{d}, \quad (6)$$

where $n^{\alpha\beta} \mathbf{a}_\beta$ is the in-plane component. The in-plane tensor $n^{\alpha\beta}$ is nevertheless not work-conjugate to the surface stretch measure $a_{\alpha\beta}$. Following the development in Naghdi¹⁸ and Simo and Fox²⁷ we introduce the work-conjugate stress resultants $\tilde{\mathbf{n}} = \tilde{n}^{\alpha\beta} \mathbf{a}_\alpha \otimes \mathbf{a}_\beta$ and the shear resultant $\tilde{\mathbf{q}} = \tilde{q}^\alpha \mathbf{a}_\alpha$. In terms of these variables, the weakform of the equilibrium equations is given as

$$\int_{\mathcal{A}} \left[\frac{1}{2} \tilde{n}^{\alpha\beta} \delta a_{\alpha\beta} + \tilde{m}^{\alpha\beta} \delta \kappa_{\alpha\beta} + \tilde{q}^\alpha \delta \gamma_\alpha \right] d\mu - G_{\text{ext}}(\delta\boldsymbol{\psi}) = 0, \quad (7)$$

where $\delta\boldsymbol{\psi}$ denotes an admissible variation to the current configuration, \mathcal{A} is the current surface area, $d\mu = \|\mathbf{a}_1 \times \mathbf{a}_2\| d\xi^1 d\xi^2 = \sqrt{a} d\xi^1 d\xi^2$ is the area element, and $G_{\text{ext}}(\delta\boldsymbol{\psi})$ is the virtual work done by external force and moment.

The shell theory is completed upon introducing constitutive equations which relate the resultant tensors $(\tilde{n}^{\alpha\beta}, \tilde{m}^{\alpha\beta}, \tilde{q}^\alpha)$ to the strain variables $(\varepsilon_{\alpha\beta}, \rho_{\alpha\beta}, \delta_\alpha)$. The constitutive equations used in this study will be presented later. The physical in-plane resultant $n^{\alpha\beta}$ is related to $\tilde{n}^{\alpha\beta}$ and $\tilde{m}^{\alpha\beta}$, and can be backed out in postprocess computations. The formula is omitted here; interested readers are referred to Simo and Fox²⁷ for details.

Forward and Inverse Analyses

This weak form (7) facilitates both the forward and the inverse solution. In the forward analysis, the reference configuration is given while current configuration is sought. The kinetic variables $(\tilde{n}^{\alpha\beta}, \tilde{m}^{\alpha\beta}, \tilde{q}^\alpha)$ are treated as functions of the deformation measures $(a_{\alpha\beta}, \kappa_{\alpha\beta}, \gamma_\alpha)$,

which in turn depend on the deformed configuration in question. Upon introducing the finite element approximation, the weak form gives rise to a set of algebraic equations for the nodal values of the deformed mid-surface position and directors. The details of the forward element formulation are contained in the seminal papers by Simo *et al.*^{26–29} This family of elements utilize a geometrically exact representation for the rotation update, and consequently they can handle arbitrarily large rotations. The element has been applied in biomechanical studies. In Kim *et al.*,^{9,10} the stress resultant shell with experimentally derived nonlinear material model were used to simulate the dynamic motion of prosthetic heart valves.

The inverse solution pursues exactly the opposite of the forward analysis. The kinetic variables $(\tilde{n}^{\alpha\beta}, \tilde{m}^{\alpha\beta}, \tilde{q}^\alpha)$ are regarded as functions of the referential measures $(A_{\alpha\beta}, K_{\alpha\beta}, \Gamma_\alpha)$, which are functions of the initial configuration. Upon introducing finite element approximation, the weak form gives rise to a set of nonlinear equations for the initial nodal positions and directors, which are subsequently solved. Once the initial mid-surface positions and directors are determined, the strain and curvatures are computed, with which the stress resultant, the stress couple, and the transverse shear stress are computed from the constitutive equations.

This inversed paradigm of stress analysis builds on a fundamental characteristic of an elastic system, that is, the stress depends on the relative deformation from the initial to the current configuration. If either of these configurations is given together with the load, the other can be determined from equilibrium. The inverse analysis applies to both continuum and structure analysis. For structural problems additional kinematic and kinetic assumptions are introduced, but the fundamental premise of reversibility remains intact.

The inverse shell element in Zhou and Liu³² utilized the same mathematical formulation for kinematics, in particular the rotation description, of the forward shell element. As a result, the inverse element can exactly revert the deformations predicted by the forward analysis. The element was developed within the framework of FEAP, a nonlinear finite element program initially developed at the University of California, Berkeley.³⁰ The inverse shell formulation is described in Zhou and Liu,³² and the details are omitted here.

Material Model

In the direct shell theory, properly invariant constitutive equations are defined in terms of the referential resultants

$$\tilde{\mathbf{N}} := J \tilde{n}^{\alpha\beta} \mathbf{A}_\alpha \otimes \mathbf{A}_\beta, \quad \tilde{\mathbf{Q}} := J \tilde{q}^\alpha \mathbf{A}_\alpha, \quad \tilde{\mathbf{M}} := J \tilde{m}^{\alpha\beta} \mathbf{A}_\alpha \otimes \mathbf{A}_\beta, \quad (8)$$

where $J = \frac{\|\mathbf{a}_1 \times \mathbf{a}_2\|}{\|\mathbf{A}_1 \times \mathbf{A}_2\|} = \sqrt{\frac{\det(a_{\alpha\beta})}{\det(A_{\alpha\beta})}}$ is the area stretch. The standard argument involving the balance of mechanical power shows that these variables are work-conjugate to the deformation measures in (4), viz.

$$\begin{aligned} \tilde{N}^{\alpha\beta} &= \frac{\partial\psi}{\partial\varepsilon_{\alpha\beta}} = 2 \frac{\partial\psi}{\partial a_{\alpha\beta}}, & \tilde{Q}^\alpha &= \frac{\partial\psi}{\partial\delta_\alpha} = \frac{\partial\psi}{\partial\gamma_\alpha}, \\ \tilde{M}^{\alpha\beta} &= \frac{\partial\psi}{\partial\rho_{\alpha\beta}} = \frac{\partial\psi}{\partial\kappa_{\alpha\beta}}, \end{aligned} \quad (9)$$

where ψ is the strain energy per unit undeformed surface.

The strain energy ψ consists of contributions from the in-plane stretching, the flexure, and the transverse shear. The in-plane properties of thin tissues are relatively easy to characterize, and considerable research has been devoted to the experimental determination of the membrane energy function of various thin tissues, e.g., Humphrey *et al.*^{6,7} and Sacks.¹⁹ In contrast, the flexure properties are difficult to determine experimentally. Only recently the bending properties of some tissues have been investigated¹⁷ and incorporated into shell models.⁹ Given the difficulty in obtaining the bending properties, a common treatment is to derive approximately the bending contribution from a known in-plane constitutive equation. This approach often leads to a decoupled energy form

$$\psi = \psi_m + \psi_b + \psi_s, \quad (10)$$

where ψ_m , ψ_b , and ψ_s corresponds to the membrane, bending, and transverse shear energies respectively. Deriving energetically consistent bending energy from in-plane constitutive equation has been an area of interest in nonlinear shell mechanics.^{20,25} Among many attempts, Schieck *et al.*²⁰ showed that the bending energy can be consistently approximated by

$$\psi_b = \frac{h^2}{24} H^{\alpha\beta\delta\gamma} \rho_{\alpha\beta} \rho_{\delta\gamma}, \quad (11)$$

where $\mathbb{H} = H^{\alpha\beta\delta\gamma} \mathbf{A}_\alpha \otimes \mathbf{A}_\beta \otimes \mathbf{A}_\delta \otimes \mathbf{A}_\gamma$ is the elasticity tensor at the ground state (i.e., when $\boldsymbol{\varepsilon} = \mathbf{0}$),

$$H^{\alpha\beta\delta\gamma} := 4 \frac{\partial^2 \psi_m}{\partial a_{\alpha\beta} \partial a_{\delta\gamma}} \Big|_{\boldsymbol{\varepsilon}=\mathbf{0}}. \quad (12)$$

The shear strain energy ψ_s is regarded as a penalty function for approximately enforcing the Kirchhoff-Love assumption.

In what follows we introduce the constitutive construction used in the present study. Seshaiyer *et al.*^{21,22} showed that a Fung-type nonlinear constitutive model describes well the in-plane stress-strain response of cerebral aneurysm wall. The Fung energy function assumes the form

$$\begin{aligned} \psi_m &= c(e^Q - 1), \\ Q &= d_1 E_{11}^2 + d_2 E_{22}^2 + 2d_3 E_{11} E_{22} + d_4 E_{12}^2, \end{aligned} \quad (13)$$

where $E_{\alpha\beta}$ represents the physical components of the Green-Lagrangian strain relative to a local Cartesian basis that aligns with the orthogonal symmetry axes ($\mathbf{E}_1, \mathbf{E}_2$) in the initial configuration. By assumption, \mathbf{E}_1 coincides with the preferred fiber direction in the initial configuration, which is written as $\mathbf{E}_1 = \tau^\alpha \mathbf{A}_\alpha$ in the convected basis. In the current configuration, the fiber direction becomes $\mathbf{e}_1 = \tau^\alpha \mathbf{a}_\alpha$. Since \mathbf{E}_1 is not known in the inverse analysis, it is convenient to use the invariant form of the energy function, so that the function can be used once the current fiber direction is given. To this end, introduce the strain invariants

$$\begin{aligned} I_1 &= \text{tr } \mathbf{C} = a_{\alpha\beta} A^{\alpha\beta}, & I_2 &= \det \mathbf{C} = \frac{\det a_{\alpha\beta}}{\det A_{\alpha\beta}}, \\ I_4 &= \frac{\tau^\alpha a_{\alpha\beta} \tau^\beta}{\tau^\delta A_{\delta\gamma} \tau^\gamma}, \end{aligned} \quad (14)$$

where I_1 and I_2 are the principal invariants of \mathbf{C} and I_4 is the squared stretch of a material line element along the preferred direction. In terms of the invariants, one has

$$\begin{aligned} E_{11} &= \frac{1}{2}(I_4 - 1), & E_{22} &= \frac{1}{2}(I_1 - I_4 - 1), \\ E_{12}^2 &= I_1 I_4 - I_4^2 - I_2. \end{aligned} \quad (15)$$

Therefore,

$$\begin{aligned} Q &= \frac{1}{4} d_2 I_1^2 + \frac{1}{4} (d_1 + d_2 - 2d_3 - 4d_4) I_4^2 \\ &\quad + \frac{1}{2} (d_3 - d_2 + 2d_4) I_1 I_4 - d_4 I_2 - \frac{1}{2} (d_2 + d_3) I_1 \\ &\quad - \frac{1}{2} (d_1 - d_2) I_4 + \frac{1}{4} (d_1 + d_2 + 2d_3). \end{aligned} \quad (16)$$

This gives the following tension function:

$$\begin{aligned} \tilde{N}^{\alpha\beta} &= ce^Q [(d_2 I_1 + (d_3 - d_2 + 2d_4) I_4 - d_2 - d_3) A^{\alpha\beta} \\ &\quad - 2d_4 I_2 a^{\alpha\beta} + [(d_1 + d_2 - 2d_3 - 4d_4) I_4 \\ &\quad + (d_3 - d_2 + 2d_4) I_1 - d_1 + d_2] (\tau^\delta A_{\delta\gamma} \tau^\gamma)^{-1} \tau^\alpha \tau^\beta]. \end{aligned} \quad (17)$$

The above derivation used the relations $\frac{\partial I_1}{\partial a_{\alpha\beta}} = A^{\alpha\beta}$, $\frac{\partial I_2}{\partial a_{\alpha\beta}} = I_2 a^{\alpha\beta}$, and $\frac{\partial I_4}{\partial a_{\alpha\beta}} = \frac{\tau^\alpha \tau^\beta}{\tau^\delta A_{\delta\gamma} \tau^\gamma}$.

For this model, the material Hessian at the zero-stress state is

$$\begin{aligned} H^{\alpha\beta\delta\gamma} &= 2c [(d_2 - 2d_4) A^{\alpha\beta} A^{\delta\gamma} \\ &\quad + d_4 (A^{\alpha\delta} A^{\beta\gamma} + A^{\alpha\gamma} A^{\beta\delta}) \\ &\quad + (d_3 - d_2 + 2d_4) (\tau^\delta A_{\delta\gamma} \tau^\gamma)^{-1} (A^{\alpha\beta} \tau^\delta \tau^\gamma + \tau^\alpha \tau^\beta A^{\delta\gamma}) \\ &\quad + (d_1 + d_2 - 2d_3 - 4d_4) (\tau^\delta A_{\delta\gamma} \tau^\delta)^{-2} \tau^\alpha \tau^\beta \tau^\delta \tau^\gamma]. \end{aligned} \quad (18)$$

The associated bending energy is given as

$$\begin{aligned}\psi_b &= \frac{h^2}{24} H^{\alpha\beta\delta\gamma} \rho_{\alpha\beta} \rho_{\delta\gamma} \\ &= \frac{h^2 c}{12} \left[(d_2 - 2d_4) (\text{tr} \boldsymbol{\rho})^2 + 2d_4 (\text{tr}(\boldsymbol{\rho}^2)) \right. \\ &\quad \left. + 2(d_3 - d_2 + 2d_4) \rho_\tau \text{tr} \boldsymbol{\rho} \right. \\ &\quad \left. + (d_1 + d_2 - 2d_3 - 4d_4) \rho_\tau^2 \right].\end{aligned}\quad (19)$$

For relatively large deformation, the use of material tangent at ground state clearly underestimates the bending stiffness. As a remedy, we introduced an amplifying correction factor f , such that $\tilde{M}^{\alpha\beta} = f \frac{\partial \psi_b}{\partial \kappa_{\alpha\beta}}$. It follows that

$$\tilde{M}^{\alpha\beta} = \frac{f h^2}{12} H^{\alpha\beta\delta\gamma} \rho_{\delta\gamma}. \quad (20)$$

For the transverse shear, we assume ψ_s can be represented as a function of scalar invariants

$$\psi_s = \frac{G_1}{2} \delta_\alpha A^{\alpha\beta} \delta_\beta + \frac{G_2}{2} (\delta_\alpha \tau^\alpha)^2 \quad (21)$$

where G_1 and G_2 are the material shear modulus. Using Eq. (9), the shear resultant is derived as:

$$\tilde{Q}^\alpha = G_1 A^{\alpha\beta} \delta_\beta + G_2 \tau^\alpha \tau^\beta \delta_\beta. \quad (22)$$

RESULTS

Stress Analysis of a Patient-Specific Cerebral Aneurysm

The aneurysm model considered here was originally constructed in the study by Ma *et al.*¹⁵ The original mesh contains large portion of regular vascular structures. Here, we remove most of the vasculature and retain only short segment of arteries connecting to the lesion. The remaining structure is remeshed to attain better element quality. The ensuing mesh is shown in Fig. 1. Although not reported here, we have performed convergence analysis on a refined grid (by subdividing the triangles) and the stress results were nearly identical. Therefore, the current mesh size was found adequate.

The surface mesh is taken to be the deformed mid-surface under 100 mmHg pressure. The director vector \mathbf{d} at each node is computed as the average of normal vectors of the adjacent elements. For the boundary condition, the edges of the vasculature are fixed. We have considered other types of boundary conditions (for example, partially free edges allowing displacement along some pre-defined directions) and confirmed that the boundary conditions only affect the stress distribution in nearby regions in the vasculature. The

influence on the stress distribution in the sac is very small.

The inverse analysis is carried out for a Fung material model presented in ‘‘Material model’’ section. The membrane energy for the Fung model is given in Eq. (13) with baseline parameters adapted from Seshaiyer *et al.*²²:

$$\begin{aligned}c &= 0.016 \text{ N/mm}, \quad d_1 = 14.50, \quad d_2 = 15.28, \\ d_3 &= 7.57, \quad d_4 = 4.96.\end{aligned}$$

Note that the Fung function (13) is energy per unit surface area, and therefore the parameter c has the dimension of force per unit length. In the aneurysm model the current preferred direction is assumed to be tangent to the surface and parallel to the horizontal plane at every material point. The associated bending constitutive model is given in Eq. (19) with the amplifying correction factor $f = 1.57$, which assumes the value of e^Q evaluated at a bi-axial strain $E_{11} = E_{22} = 0.1$. Note that the inverse shell analysis outputs the stress resultant $\tilde{\mathbf{n}}$. The in-plane membrane stress is computed by

$$\sigma^{\alpha\beta} = \frac{\tilde{n}^{\alpha\beta}}{h}. \quad (23)$$

Here, due to the lack of knowledge about the wall thickness, a uniform value of $h = 0.1$ mm is assumed.

The predicted initial configuration is shown in Fig. 1 superposed on the imaged mesh. The membrane stress in the deformed configuration are shown in Fig. 2. The large membrane stress happens near the (flatter) shoulder area and the (saddle) root regions.

In Fig. 3, the transverse shear stress norm, defined as $q = \frac{\sqrt{(\tilde{q}^1)^2 + (\tilde{q}^2)^2}}{h}$, is shown. In the sac region, the transverse shear stress norm is mostly below 0.05 N/mm², which is much smaller than membrane stress. At several scattered points the shear stress is slightly higher, around 0.1 N/mm². Near the fixed boundary, the transverse shear is much larger, with the maximum value close to 1.0 N/mm². However, the high shear stress is restricted to a narrow boundary layer.

The norm of the stress couple $M = \sqrt{M_1^2 + M_2^2}$ (M_1 and M_2 are the principal couples) is shown in Fig. 4. Clearly, larger stress couple happens at areas where the lesion experiences significant curvature change. A larger value in the stress couple indicates significant stress variation across the thickness. Note that the M is the stress couple per unit length, thus bears the unit of force.

Material Sensitivity Analysis

Evaluating the sensitivity of stress solution to material parameters is an important task for aneurysm

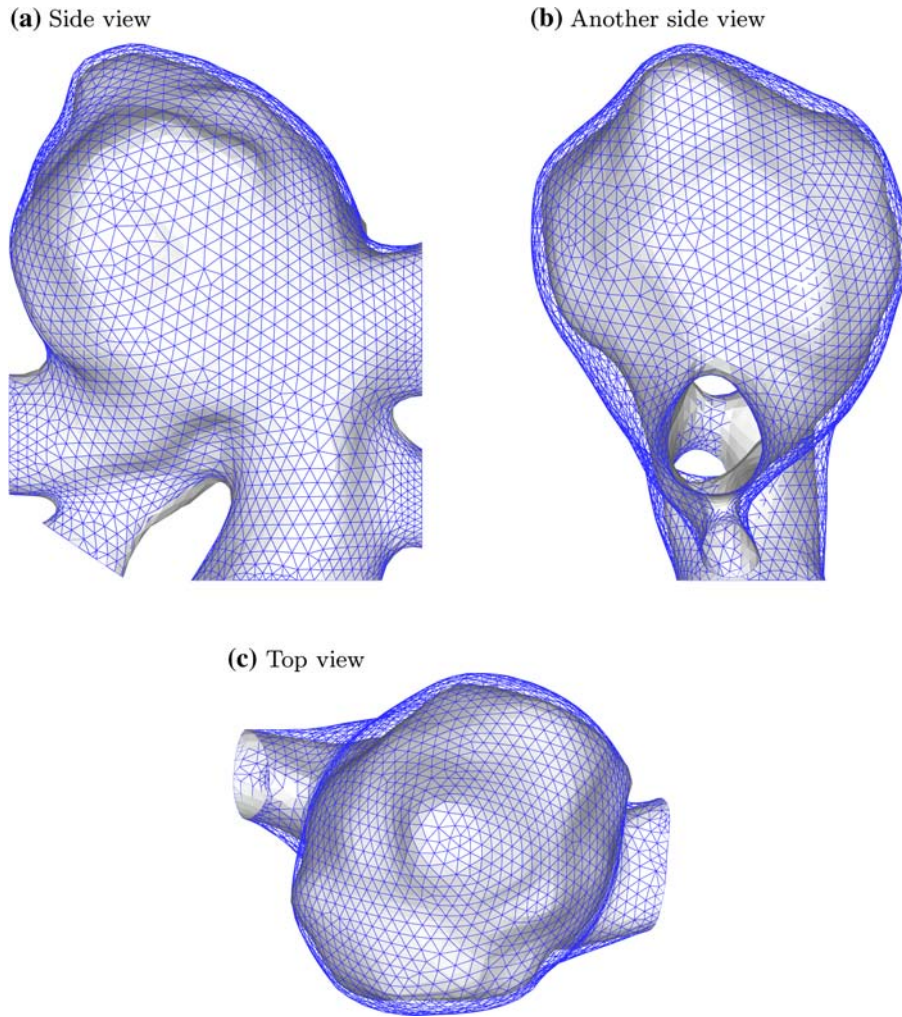


FIGURE 1. Views of the stress-free configuration of a pressurized cerebral aneurysm predicted by the inverse shell approach. The predicted initial geometry (shaded) is visibly smaller than the *in vivo* shape (mesh). In the FE model, the nodes at the boundary edges are fixed.

stress analysis, because currently it is impractical to obtain and apply patient-specific tissue properties. For pressurized conduit-like structures, the in-plane stress resultant should depend primarily on the geometry and load, although the influence of material parameters presents in regions near boundary constraints. In Lu *et al.*,¹⁴ we have demonstrated numerically a lack of material influence in a membrane model of cerebral aneurysm. In this section, we will examine the material sensitivity in the inverse shell analysis.

The inverse shell analyses are carried out on the cerebral aneurysm for two family of materials. Within each family, the material constants are varied to create two sub-models. The baseline model for the first family is the Fung model used in “[Stress analysis of a patient-specific cerebral aneurysm](#)” section. The sub-model in this family is generated by magnifying the stiffness parameter c 100 times. The second family is modeled

after the isotropic Mooney-Rivlin material, which is an isotropic hyperelastic function. This material is introduced to signify that even models with incorrect symmetry description may lead to close stress prediction. The membrane energy density for this material takes the form

$$\psi_m = \frac{\mu_1}{2}(I_1 - 2 \log J - 2) + \frac{\mu_2}{2}(I_2 - 2 \log J - 1), \quad (24)$$

where μ_1 and μ_2 are material parameters. The baseline parameters are

$$\mu_1 = 0.16 \text{ N/mm}, \quad \mu_2 = 0.1872 \text{ N/mm}.$$

The numbers are obtained by fitting the averaged isotropic parameters in Seshaiyer *et al.*²² to the Mooney-Rivlin model. The other model in this family is defined by magnifying the parameter μ_1 and μ_2 100 times.

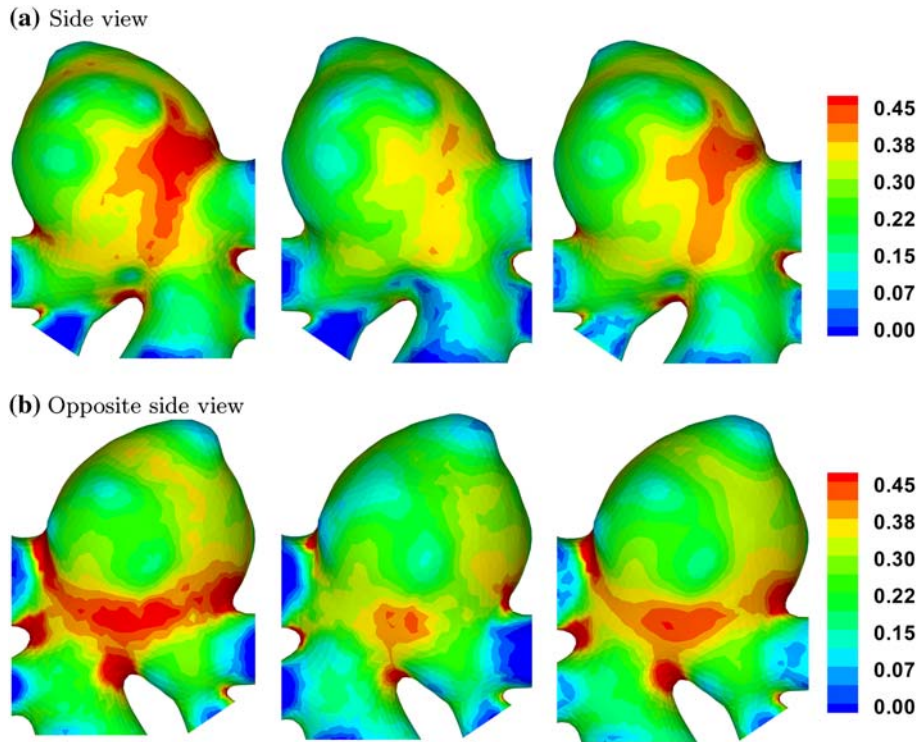


FIGURE 2. Predicted principal stresses from the shell model with a Fung material. From left to right: the first principal membrane stress; the second principal membrane stress; the von Mises membrane stress. Unit of stress: N/mm^2 .

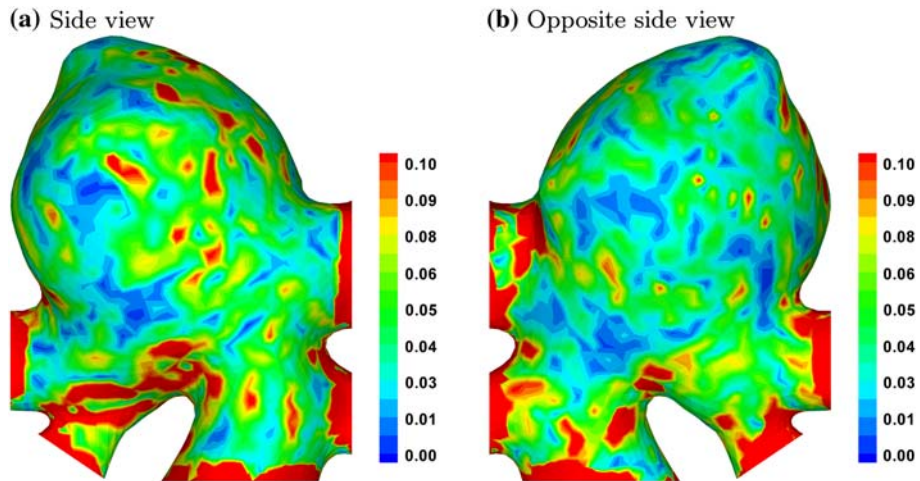


FIGURE 3. Distribution of the shear stress norm. Unit: N/mm^2 .

The Mooney-Rivlin model gives the following tension function:

$$\tilde{N}^{\alpha\beta} = \mu_1 A^{\alpha\beta} - (\mu_1 + \mu_2 - \mu_2 I_2) a^{\alpha\beta}. \quad (25)$$

The ground state elasticity tensor of the membrane energy function in Eq. (12) is obtained as

$$H^{\alpha\beta\delta\gamma} = \mu_1 (A^{\alpha\delta} A^{\beta\gamma} + A^{\alpha\gamma} A^{\beta\delta}) + 2\mu_2 A^{\alpha\beta} A^{\delta\gamma}. \quad (26)$$

The associated bending energy is characterized by

$$\psi_b = \frac{h^2}{24} H^{\alpha\beta\delta\gamma} \rho_{\alpha\beta} \rho_{\delta\gamma} = \frac{h^2}{12} [\mu_2 (\text{tr} \boldsymbol{\rho})^2 + \mu_1 \text{tr}(\boldsymbol{\rho}^2)]. \quad (27)$$

It follows that

$$\tilde{M}^{\alpha\beta} = \frac{h^2}{6} [\mu_1 A^{\alpha\delta} \rho_{\delta\gamma} A^{\beta\gamma} + \mu_2 (\text{tr} \boldsymbol{\rho}) A^{\alpha\beta}]. \quad (28)$$

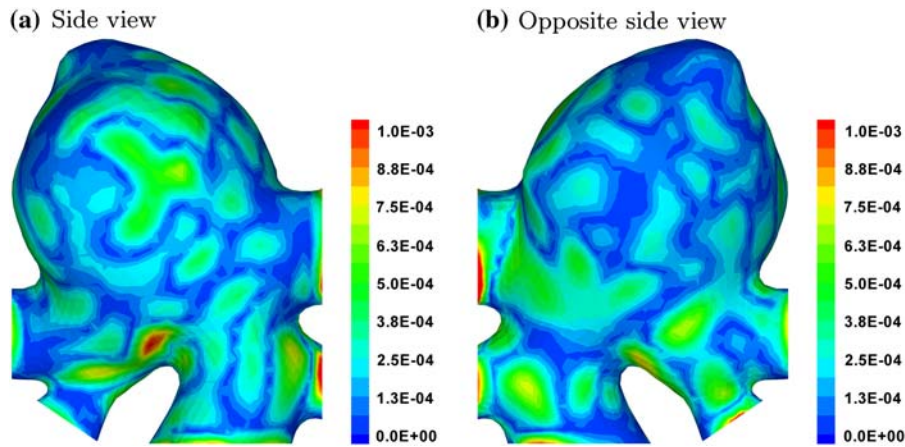


FIGURE 4. Distribution of the stress couple. Unit: N (torque per unit length).

The transverse shear constitutive equation is specified in Eq. (22). Due to isotropy, $G_2 = 0$. We assume $G_1 = \mu_1 + \mu_2$.

The initial configuration predicted with the baseline Mooney-Rivlin material is comparable to the one obtained with the baseline Fung material, while for the stiff models the deformation is very small. Figure 5 presents the principal stresses distributions (top view) for all four material models. Despite the difference in material properties, the predicted stress distributions appear very close for all cases.

In Fig. 6, the percentage stress difference between the baseline Mooney-Rivlin model and the baseline Fung model is plotted. In order to avoid the stress difference being divided by very small number, here the stress difference is divided by a reference value 0.3 N/mm^2 , which is close to the maximum stress value in the sac region. As seen from the figure, in the sac region the relative stress difference is mostly below 3%. Away from the sac, the difference elevates while the maximum difference occurs near the boundary due to boundary effects.

DISCUSSIONS

Comparison of Stress Solution with Other Models

In the sac region, as shown in the corresponding top view in Fig. 5a, the von Mises stress mostly ranges from 0.11 to 0.36 N/mm^2 . The maximum stress appears larger than that from the membrane analysis,¹⁴ which predicted a maximum membrane stress of approximately 0.30 N/mm^2 . The difference in these two models may be attributed to the different surface characteristics. In the membrane model, the concave and locally flat regions are artificially removed, resulting a smoother surface. Nevertheless, the distributions are

very similar. In particular, the high stress regions around the shoulder are captured in both models. Compared to the forward analysis by Ma *et al.*,¹⁶ in which the same cerebral aneurysm but only the sac was analyzed (with a finer mesh), the inverse stresses appear to be uniformly smaller. This is expected, because the forward analysis adds an artificial distension to the *in vivo* configuration and result in a larger radius. The maximum von Mises stress in Ma *et al.*¹⁶ was 0.52 N/mm^2 . It should be noted that the model in Ma *et al.*¹⁶ assumed a wall thickness of 0.086 mm , which is smaller than the thickness of 0.1 mm used in this analysis. Moreover, the stress value in Ma *et al.*¹⁶ also includes the bending contribution whereas the current computation does not. Considering the thickness difference, the stress value should be scaled down to $0.52 \times 0.86 = 0.45 \text{ N/mm}^2$. The scaled maximum stress is approximately 30% greater than the inverse prediction. If the bending contribution is considered the difference is expected to be smaller. This over stress pattern is in agreement with our previous investigation on an abdominal aortic aneurysm (AAA),¹³ in which we observed that the forward analysis over-predicted the stresses.

In overall, the stress distributions predicted from the shell model with forward analysis in Ma *et al.*,¹⁶ the membrane model with modified surface characteristic,¹⁴ and the present inverse shell model are in good agreement. In all three models, large membrane stress occurs at the flatter regions near the shoulder. The deformation in this region is likely dominated by membrane stretching. Therefore, as in the membrane model,¹⁴ the wall stress is directly related to the local surface curvature, and a relatively flatter surface (smaller curvature) gives higher stress. The current model, which includes short segments of the regular vasculature, further reports high stress near the lesion root. Since the stress is simply computed by dividing

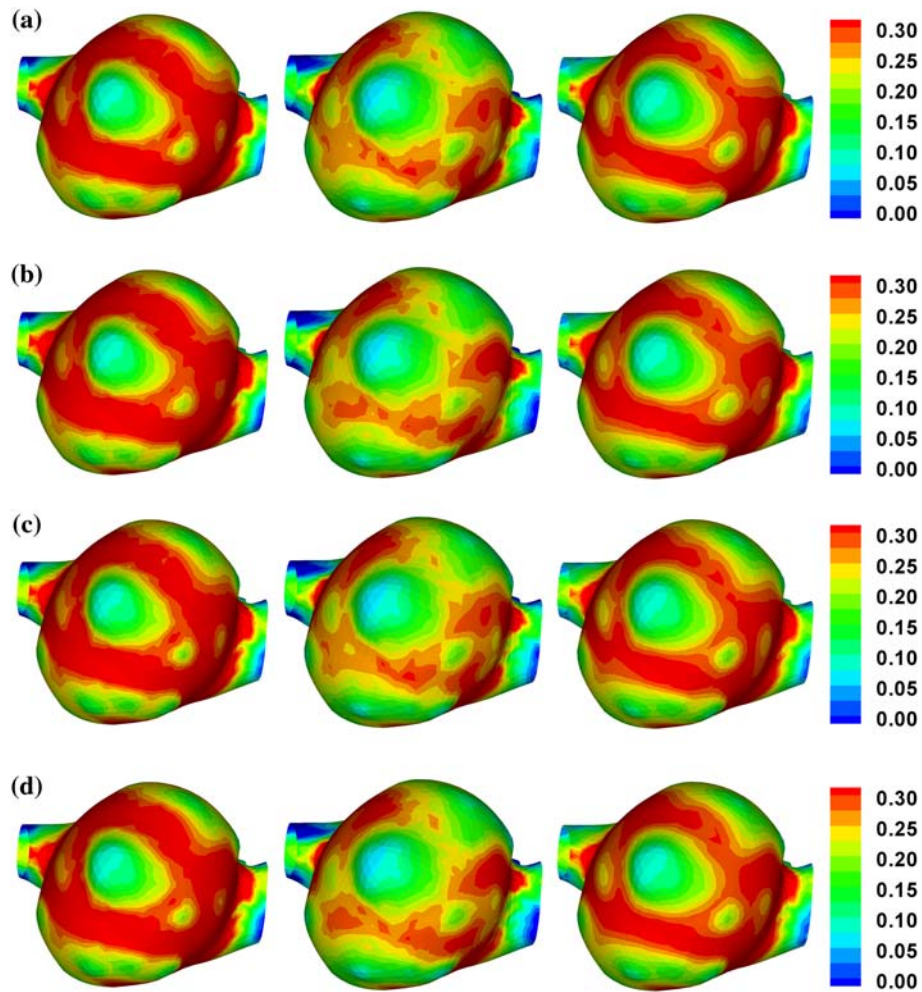


FIGURE 5. Comparative stress distributions from the Fung models and the Mooney-Rivlin models. Unit of stress: N/mm^2 . (a) Principal stresses in the baseline Fung model (c , d_1 , d_2). From left to right: the first principal membrane stress; the second principal membrane stress; the von Mises membrane stress. (b) Principal stresses in the stiff Fung model ($100c$, d_1 , d_2). (c) Principal stresses stress in the baseline Mooney-Rivlin model (μ_1 , μ_2). (d) Principal stresses in the stiff Mooney-Rivlin model ($100\mu_1$, $100\mu_2$).

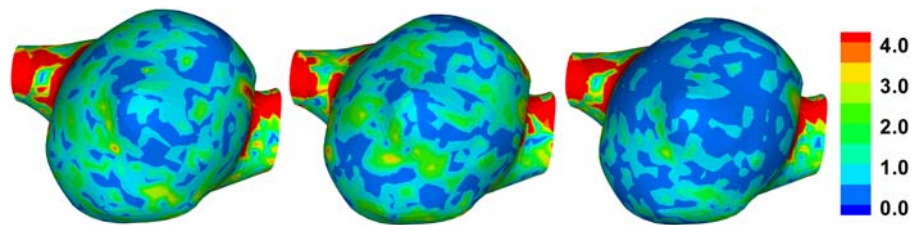


FIGURE 6. The percentage of the stress difference between the Mooney-Rivlin model (μ_1 , μ_2) and the baseline Fung model (c , d_1 , d_2) relative to a reference value 0.3 N/mm^2 . From left to right: the percentage difference in the first principal membrane stress, the second principal membrane stress, and the von Mises membrane stress.

the resultant with the thickness, a high tension in the root does not mean the rupture will most likely happen there, because in reality the wall at root is typically thicker than that of the dome region. Moreover, the material strength in the dome region is in general weaker due to the degeneration of the lesion wall.

Stress Couple

In the stress resultant theory, the stress couple is a measure of stress variations over the thickness. If we assume that the stress varies linearly across the thickness, the stress distribution across the thickness can be

determined once the stress resultant and the stress couple are found, in the same manner as the linear shell theory. It should be noted that the linear variation is not a valid assumption for nonlinear shells undergoing large deformation. For this reason, we did not compute the over-thickness distribution. Thus, the stress reported here is the membrane stress only, that is, the cross-thickness average. Nevertheless, it is informative to estimate the contribution of the stress couple to the total stress. To this end, we use a simple beam analogy. If we regard the stress couple norm M as the bending moment per unit width acting on a beam of height h , the bending stress is on the order of $\frac{M}{h}$. As seen from Fig. 4, the value of M over the sac region ranges from 0 to 4.0×10^{-4} N. The average is 2.25×10^{-4} N. The average von Mises membrane stress is 0.248 N/mm². In terms of the averages the bending contribution is on the order of $2.25 \times 10^{-4}/0.1^2 = 0.0225$ N/mm², which is one order smaller than the membrane stress in the same region. We conclude that for this cerebral aneurysm the membrane stretch dominates bending in the sac region.

Sensitivity

As pointed out in a previous study,¹⁴ the static determinacy of stress in membrane theory hinges on the fact the equilibrium equations form a closed system for solving the stress resultant (there are three differential equations for three stress components). Therefore, for membranes subject to traction boundary condition the stress can be determined from equilibrium alone. Even with the presence of displacement constraints, if the membrane is sufficiently deep, the boundary effect is expected to exist only in a thin boundary layer. However, this argument does not apply to the shell theory. In the shell theory, the equilibrium equations take the form

$$\begin{aligned} \frac{1}{\sqrt{a}}(\sqrt{a}\mathbf{n}^\alpha)_{,\alpha} + \bar{\mathbf{n}} &= \mathbf{0}, \\ \frac{1}{\sqrt{a}}(\sqrt{a}\mathbf{d} \times \tilde{\mathbf{m}}^\alpha)_{,\alpha} + \mathbf{a}_\alpha \times \mathbf{n}^\alpha + \bar{\mathbf{m}} &= \mathbf{0}, \end{aligned} \quad (29)$$

where $\bar{\mathbf{n}}$ and $\bar{\mathbf{m}}$ are the resultants of external loads. A close examination at the shell balance equation (29) shows that these tension components can not be determined by the balance equations alone. Considering only the three component equations of Eq. (29)₁, there are six unknown stress components, which include four components from the membrane resultant tensor ($n^{\alpha\beta}$ and $n^{12} \neq n^{21}$ in general) and two components from the shear resultant (\tilde{q}^α). Obviously, without introducing the material model and boundary conditions, the equations are not closed.

Nonetheless, if the bending moment and transverse shear are much smaller when compared to the membrane stresses, the shell balance equations should approach the same static determinacy. In order to explain the material insensitivity, let's re-examine the shell balance equation (29)₁ and the stress distribution in the cerebral aneurysm sac region. If the stress couple is very small (compared to the stress resultant times the wall thickness), approximately $n^{\alpha\beta} = \tilde{n}^{\alpha\beta}$, rendering the symmetry of $n^{\alpha\beta}$. It is the case for the sac region since the value of stress couple (on the order of 10^{-4}) is one order smaller than the membrane resultant multiplying the wall thickness (on the order of 10^{-3}). Furthermore, as shown in Fig. 3, in the sac region the transverse shear stress is much smaller than the membrane stress except a few scattered locations. Therefore, only the three membrane stress components (n^{11} , n^{22} , and $n^{12} \approx n^{21}$) are significant for the shell balance equation (29)₁, which gives three components equations. Apparently, this observation explains the material insensitivity seen in the cerebral aneurysm sac region.

Strain and Material Property

In this study, the strain is not reported. Obviously, the material parameters have a significant effect on the strain. For example, the stiff Fung models used give very small deformation while large deformation is observed for more compliant models. Although the results from this paper suggest that the stress resultant may be predicted accurately even with nonrealistic material properties, the accurate material properties are imperative if the strain, or equivalently the initial configuration, or the stress at a different pressure, are sought. If material properties are indeed known, then this method can accurately determine the initial stress-free configuration and hence, strain distribution also. But perhaps the most exciting outcome of this body of work is its implication to *in vivo* material property estimation. With the advent of dynamic imaging, it may be possible to accurately obtain the aneurysm configuration under several different pressures. The inverse method would then be ideal for reverse-estimating the material model for the aneurysm wall using the known strain distributions allowing for patient-specific, noninvasive assessments of material wall caliber. Towards this end a general framework has been proposed^{8,31} to utilize the inverse stress analysis for noninvasive characterization of thin-walled structures.

Limitations

A major limitation in this study is the assumption on thickness. Due to lack of knowledge of the wall

thickness, a uniform thickness is assumed based on reported values. Although the stress resultant $\bar{\mathbf{n}}$ is found to depend primarily on the load and the deformed geometry, the membrane stress, computed from (23), depends inversely on the thickness. Therefore, the stress is not accurate without knowing the wall thickness. If the thickness varies from point to point, the stress resultant should still remain insensitive to all the material parameters. However, the stress should be computed with the local thickness value. It should also be noted that the thickness has a nontrivial influence on the stress couple. Without knowledge of the actual wall-thickness, the stress couple can not be accurately predicted. This limitation can not be addressed numerically; hopefully, it will be eliminated with the improvement of imaging or other *in vivo* measurement technology.

Another limitation in this work relates to our treatment of bending constitutive equation. In the stress resultant shell theory, both the in-plane stress-strain relation and the bending-curvature relations need to be specified. While this constitutive approach opens the possibility of independently characterizing the in-plane and flexure properties, in most cases only the in-plane properties were characterized due to the difficulties of thin-tissue bending test. In this work, we employed the best-known model^{21,22} for the in-plane response. The bending response was derived from the in-plane function through the reduction procedure proposed by Schieck *et al.*,²⁰ thus bringing another modeling error. The bending-curvature relation derived in this manner is valid for small to moderately large rotations. Nevertheless, this constitutive approach is adequate for deformations where membrane stretch dominates bending. For cerebral aneurysms, we expect that the bending constitutive equation, while critical to bending prediction, would have a limited influence on the in-plane membrane stress due to the thinness of the structure.

In the constitutive theory, the shear strain energy ψ_s is regarded as a penalty function for approximately enforcing the Kirchhoff-Love assumption. The choice G_1 and G_2 values needs numerical experiment. In theory, if the values are sufficiently large in comparison to the in-plane stiffness parameter, the predicted mid-surface deformation should converge to a asymptotic solution in which the directors \mathbf{d} remain approximately normal to the mid-surface. We have performed numerical tests in the forward setting, in Ma *et al.*¹⁶ and Kim *et al.*⁹ It has been observed that as G_1 (G_2 was taken to be zero) increases, its influence on the mid-surface position (and therefore the in-plane stretching) becomes diminishingly small. Converged solutions were often obtained when G_1 was comparable to the major stiffness parameter (e.g., the parameter c in the

Fung model). Drawn on these experience, we did not perform parametric study on G_1 , but selected values based on the stiffness parameters. We believe that the influence on the in-plane stress is sufficiently small.

Lastly, the uniqueness of the inverse solution remains an open question. Although we did not encounter nonunique solution in the reported example, it is conceivable that multiple solutions may occur due to material instability or structural buckling. It is reasonable to expect that the uniqueness of the inverse problem is the same as that of the forward problem, but since the forward problem is only implicitly defined, the uniqueness of which is not known *a priori* and so is the inverse problem. The uniqueness issue and its effect on stress analysis need further research.

Summary

We proposed an inverse approach of stress analysis for cerebral aneurysms using the stress resultant shell model. We demonstrated that the wall stress and an initial stress-free configuration can be predicted by taking a deformed configuration and the corresponding pressure as input. For the particular aneurysm considered, we showed that the sac deformation was dominated by wall stretching, and the in-plane stress in the sac was insensitive to material model. Our work submitted a theoretically accurate way to consider the pre-deformation in aneurysm stress analysis, and suggested that for some lesions the wall stress may be estimated using assumed tissue properties without patient-specificity. The last feature is significant to patient-specific studies, since currently it is impractical to obtain patient-specific tissue properties for cerebral aneurysm.

ACKNOWLEDGMENTS

The work was funded by the National Science Foundation Grant CMS 03-48194 and the NIH(NHLBI) Grant 1R01HL083475-01A2. The supports are gratefully acknowledged.

REFERENCES

- ¹Brisman, J. L., J. K. Song, and D. W. Newell. Cerebral aneurysms. *N. Engl. J. Med.* 355:928–939, 2006.
- ²David, G., and J. D. Humphrey. Further evidence for the dynamic stability of intracranial saccular aneurysms. *J. Biomech.* 36:1143–1150, 2003.
- ³Elger, D. F., D. M. Blackletter, R. S. Budwig, and K. H. Johansen. The influence of shape on the stresses in model abdominal aortic aneurysms. *J. Biomech. Eng. Trans. ASME* 118:326–332, 1996.

- ⁴Humphrey, J. D., and P. B. Canham. Structure, mechanical properties, and mechanics of intracranial saccular aneurysms. *J. Elast.* 61:49–81, 2000.
- ⁵Humphrey, J. D., and S. K. Kyriacou. The use of laplace's equation in aneurysms mechanics. *Neurol. Res.* 18:204–208, 1996.
- ⁶Humphrey, J. D., R. K. Strumpf, and F. C. P. Yin. Determination of a constitutive relation for passive myocardium. I. A new functional form. *ASME J. Biomech. Eng.* 112(3):333–339, 1990.
- ⁷Humphrey, J. D., R. K. Strumpf, and F. C. P. Yin. Determination of a constitutive relation for passive myocardium. II. Parameter-estimation. *ASME J. Biomech. Eng.* 112(3):340–346, 1990.
- ⁸Lu, J., and X. Zhao. Pointwise identification of elastic properties in nonlinear hyperelastic membranes. Part I: theoretical and computational developments. *J. Appl. Mech.* 76:061013/1–061013/10, 2009.
- ⁹Kim, H., K. B. Chandran, M. S. Sacks, and J. Lu. An experimentally derived stress resultant shell model for heart valve dynamic simulations. *Ann. Biomed. Eng.* 35(1): 30–44, 2007.
- ¹⁰Kim, H., J. Lu, M. S. Sacks, and K. B. Chandran. Dynamic simulation of bioprosthetic heart valves using a stress resultant shell model. *Ann. Biomed. Eng.* 36:262–275, 2008.
- ¹¹Kyriacou, S. K., and J. D. Humphrey. Influence of size, shape and properties on the mechanics of axisymmetric saccular aneurysms. *J. Biomech.* 29:1015–1022, 1996.
- ¹²Lu, J., X. Zhou, and M. L. Raghavan. Computational method of inverse elastostatics for anisotropic hyperelastic solids. *Int. J. Numer. Methods Eng.* 69:1239–1261, 2007.
- ¹³Lu, J., X. Zhou, and M. L. Raghavan. Inverse elastostatic stress analysis in pre-deformed biological structures: demonstration using abdominal aortic aneurysm. *J. Biomech.* 40:693–696, 2007.
- ¹⁴Lu, J., X. Zhou, and M. L. Raghavan. Inverse method of stress analysis for cerebral aneurysms. *Biomech. Model. Mechanobiol.* 7:477–486, 2008.
- ¹⁵Ma, B., R. E. Harbaugh, and M. L. Raghavan. Three-dimensional geometrical characterization of cerebral aneurysms. *Ann. Biomed. Eng.* 32:264–273, 2004.
- ¹⁶Ma, B., J. Lu, R. E. Harbaugh, and M. L. Raghavan. Nonlinear anisotropic stress analysis of anatomically realistic cerebral aneurysms. *ASME J. Biomed. Eng.* 129:88–99, 2007.
- ¹⁷Mirnajafi, A., J. Raymer, M. J. Scott, and M. S. Sacks. The effects of collagen fiber orientation on the flexural properties of pericardial heterograft biomaterials. *Biomaterials* 26:795–804, 2005.
- ¹⁸Naghdi, P. M. The theory of plates and shells. In: *Handbuch der Physik*, vol. VIa/2, edited by C. Truesdell. Berlin: Springer-Verlag, 1972, pp. 425–640.
- ¹⁹Sacks, M. S. Biaxial mechanical evaluation of planar biological materials. *J. Elast.* 61:199–246, 2000.
- ²⁰Schieck, B., W. Pietraszkiewicz, and H. Stumpf. Theory and numerical analysis of shells undergoing large elastic strains. *Int. J. Solids Struct.* 29:689–709, 1992.
- ²¹Seshaiyer, P., and J. D. Humphrey. A sub-domain inverse finite element characterization of hyperelastic membranes including soft tissues. *J. Biomech. Eng. Trans. ASME* 125: 363–371, 2003.
- ²²Seshaiyer, P., F. P. K. Hsu, A. D. Shah, S. K. Kyriacou, and J. D. Humphrey. Multiaxial mechanical behavior of human saccular aneurysms. *Comput. Methods Biomed. Eng.* 4:281–289, 2001.
- ²³Shah, A. D., and J. D. Humphrey. Finite strain elastodynamics of intracranial saccular aneurysms. *J. Biomech.* 32:593–599, 1999.
- ²⁴Shah, A. D., J. L. Harris, S. K. Kyriacou, and J. D. Humphrey. Further roles of geometry and properties in the mechanics of saccular aneurysms. *Comput. Methods Biomed. Eng.* 1:109–121, 1998.
- ²⁵Simmonds, J. G. The strain energy density of rubber-like shells. *Int. J. Solids Struct.* 21:67–77, 1985.
- ²⁶Simo, J. C. On a stress resultant geometrically exact shell model. Part VII: shell intersections with 5/6-dof finite element formulations. *Comput. Methods Appl. Mech. Eng.* 108:319–339, 1993.
- ²⁷Simo, J. C., and D. D. Fox. On a stress resultant geometrically exact shell model. Part I. Formulation and optimal parametrization. *Comput. Methods Appl. Mech. Eng.* 72(3): 267–304, 1989.
- ²⁸Simo, J. C., and D. D. Fox. On a stress resultant geometrically exact shell model. Part II: the linear theory; computational aspects. *Comput. Methods Appl. Mech. Eng.* 73: 53–92, 1989.
- ²⁹Simo, J. C., D. D. Fox, and M. S. Rifai. On a stress resultant geometrically exact shell model. Part III: computational aspects of the nonlinear-theory. *Comput. Methods Appl. Mech. Eng.* 79:21–70, 1990.
- ³⁰Taylor, R. L. FEAP User Manual: v7.5. Technical Report. Berkeley: Department of Civil and Environmental Engineering, University of California, 2003.
- ³¹Zhao, X., X. Chen, and J. Lu. Pointwise identification of elastic properties in nonlinear hyperelastic membranes. Part II: experimental validation. *J. Appl. Mech.* 76:061014/1–061014/8, 2009.
- ³²Zhou, X., and J. Lu. Inverse formulation for geometrically exact stress resultant shells. *Int. J. Numer. Methods Eng.* 74:1278–1302, 2008.